

## An evaluation of ambient ammonia concentrations over southern Ontario simulated with different dry deposition schemes within STILT-Chem v0.8

Deyong Wen<sup>1</sup>, Leiming Zhang<sup>2</sup>, John C. Lin<sup>1,3</sup>, Robert Vet<sup>2</sup>, and Michael D. Moran<sup>2</sup>

<sup>1</sup>Waterloo Atmosphere-Land Interactions Research Group, Department of Earth and Environmental Sciences, University of Waterloo, Canada

<sup>2</sup>Air Quality Research Division, Science and Technology Branch, Environment Canada, Canada

<sup>3</sup>Department of Atmospheric Sciences, University of Utah, USA

*Correspondence to:* J. C. Lin (john.lin@utah.edu)

**Abstract.** A bi-directional air-surface exchange scheme for atmospheric ammonia was incorporated into the Stochastic Time-Inverted Lagrangian Transport air quality model (STILT-Chem v0.8). STILT-Chem v0.8 was then applied to simulate atmospheric ammonia concentrations at 53 measurement sites in the province of Ontario, Canada for a six-month period from 1 June to 30 November 2006. In addition to the bi-directional scheme, two uni-directional dry deposition schemes were tested. Comparisons of modeled ammonia concentrations against observations show that all three schemes can reasonably predict observations. For sites with low observed ammonia concentrations, the bi-directional scheme clearly overestimated ammonia concentrations during crop-growing season. Although all three schemes tended to underestimate ammonia concentrations after mid-October and for sites with elevated observed concentrations, mainly due to underestimated NH<sub>3</sub> emission inventory after mid-October and/or underestimated emission potentials for those sites, the bi-directional scheme performed better because of its introduction of compensation points into the flux calculation parameterization. In addition to uncertainties in the emission inventory, the results of additional sensitivity tests suggest that uncertainties in the input values of emission potentials in the bi-directional scheme greatly affect the accuracy of modeled ammonia concentrations. The use of much larger emission potentials in the bi-directional scheme and larger anthropogenic NH<sub>3</sub> emission after mid-October than provided in the model emissions files is needed for accurate prediction of elevated ammonia concentrations at intensive agricultural locations.

## 1 Introduction

20 As the primary basic gas in the atmosphere, atmospheric ammonia ( $\text{NH}_3$ ) plays an important role  
in several biogeochemical processes (Seinfeld and Pandis, 2006). It acts as a major agent in neu-  
tralizing acids in the atmosphere and substantially contributes to fine particulate matter ( $\text{PM}_{2.5}$ )  
concentrations, which have impacts on air quality, acid deposition, atmospheric visibility, and cli-  
mate. For example, human morbidity has been shown to increase linearly with  $\text{PM}_{2.5}$  concentrations  
25 (Pope et al., 2009), and excessive deposition of atmospheric  $\text{NH}_3$  and ammonium may lead to soil  
acidification and damage to sensitive species and ecosystem health (Morris, 1991; Van Bremen et al.,  
1982).

Unlike most gas-phase atmospheric species, which are predominantly either deposited to or emit-  
ted from the surface,  $\text{NH}_3$  is a semi-volatile species and exhibits bi-directional exchange between  
30 the atmosphere and the Earth's surface. However, dry deposition and emission of  $\text{NH}_3$  are simu-  
lated entirely separately in most atmospheric  $\text{NH}_3$  modeling studies (Simpson et al., 2012; Vieno  
et al., 2010; Geels et al., 2012). Such a decoupled treatment of these two processes is less realistic  
than a combined, bi-directional, gradient-driven flux model. Simulations with separate representa-  
tions of emission and dry deposition likely underestimate ambient  $\text{NH}_3$  concentrations. Thus, the  
35 development of bi-directional modeling of  $\text{NH}_3$  is important since the bi-directional approach is  
responsive to combined changes of these two processes and allows for more accurate estimation of  
surface fluxes. Significant efforts have been made in the past two decades to develop bi-directional  
 $\text{NH}_3$  flux models (Sutton et al., 1998; Nemitz et al., 2001; Wu et al., 2009; Cooter et al., 2010;  
Wichink Kruit et al., 2010, 2012; Zhang et al., 2010).

40 Most existing bi-directional flux models for  $\text{NH}_3$  were parameterized for applications at canopy  
scales (Flechard et al., 2013). Only a few models were developed for implementation in regional-  
scale air quality models due to the lack of required input parameters over a large number of different  
land-use categories (Wichink Kruit et al., 2010, 2012; Cooter et al., 2010, 2012; Bash et al., 2013;  
Pleim et al., 2013). For example, required inputs of ground and stomatal emission potentials are  
45 generally not measured at regional scales or not explicitly calculated in regional-scale models. Zhang  
et al. (2010) developed a bi-directional exchange model for  $\text{NH}_3$  that can be easily implemented in  
any regional-scale air quality model: the required inputs of stomatal and ground emission potentials  
were empirically derived for different land-use categories based on an extensive literature review.

Although bi-directional exchange models of  $\text{NH}_3$  are more mechanistically realistic in principle,  
50 few studies have examined their actual performances against uni-directional dry deposition models  
at multiple measurement sites with a variety of different levels of  $\text{NH}_3$  (Wichink Kruit et al., 2012).  
In this study, the bi-directional exchange scheme of Zhang et al. (2010) was implemented in the  
Stochastic Time-Inverted Lagrangian Transport air quality model (STILT-Chem v0.8). The model  
was then used to simulate  $\text{NH}_3$  concentrations at 53 measurement sites in southern Ontario, Canada,  
55 first with the bi-directional scheme and then with two uni-directional dry deposition schemes that had

already been included in the model. The main objective of this study was to assess the performances of these three dry deposition schemes in atmospheric  $\text{NH}_3$  modeling using a detailed data set of  $\text{NH}_3$  measurements. The uncertainties associated with using predefined emission potentials in the bi-directional scheme were also examined.

## 60 **2 Model description**

### **2.1 STILT-Chem for $\text{NH}_3$**

STILT-Chem v0.8 was employed in this study to simulate emissions, transport, transformation, and deposition of atmospheric  $\text{NH}_3$  as well as other key atmospheric species. STILT-Chem (Wen et al., 2012, 2013) is a stochastic Lagrangian air quality model developed from the Stochastic Time-  
65 Inverted Lagrangian Transport model (STILT; see <http://www.stilt-model.org>) (Lin et al., 2003). A STILT-Chem simulation begins with a stochastic back-trajectory simulation, followed by forward calculations that determine tracer concentrations along the generated back trajectories. In the back-trajectory simulation, numerous virtual particles, each representing an air parcel, are released from a receptor and transported backward in time for a specific period. Each particle is transported by  
70 both interpolated mean wind fields as well as stochastic velocities representing turbulent eddies. After back trajectories have been calculated, the concentrations of modeled species are initialized at the endpoint of each back trajectory using values output from a global chemical transport model. The initial parcel concentrations are then evolved forward in time along each trajectory to take into consideration the influences of emissions, deposition, and chemical transformation. STILT-Chem  
75 uses the Carbon Bond IV (CB4) gas-phase chemical mechanism (Gery et al., 1989) to simulate the time evolution of the concentrations of a variety of gas-phase species in the atmosphere while using an additional chemistry module to simulate the multiphase species involved in the key atmospheric reactions of atmospheric  $\text{NH}_3$  and ammonium. A comprehensive description of the treatment of emission, transport, transformation, and deposition of atmospheric  $\text{NH}_3$  and ammonium in STILT-  
80 Chem can be found in Wen et al. (2013).

### **2.2 Two uni-directional dry deposition schemes**

#### **2.2.1 Wesely dry deposition scheme**

A dry deposition scheme based on the work of Wesely (1989) (hereafter referred to as “WDD”) was used as the default in STILT-Chem to compute dry deposition velocities of the modeled gaseous and aerosol species (Draxler and Hess, 1997). The WDD scheme estimates the dry deposition velocity by utilizing the resistance analogy method (Fig. 1), in which each species-specific dry deposition

velocity ( $v_d$  in  $\text{ms}^{-1}$ ) is calculated as (Draxler and Hess, 1997)

$$v_d = (R_a + R_b + R_c + R_a R_b v_g)^{-1} + v_g \quad (1)$$

where  $R_a$  ( $\text{sm}^{-1}$ ) is the aerodynamic resistance between a specified height and the surface,  $R_b$  ( $\text{sm}^{-1}$ ) is the quasi-laminar sublayer resistance, and  $R_c$  ( $\text{sm}^{-1}$ ) is the bulk canopy surface resistance and is zero for particles.  $R_a$  ( $\text{sm}^{-1}$ ) is computed using the friction velocity and the Businger stability functions for the surface layer;  $R_b$  ( $\text{sm}^{-1}$ ) is computed in different ways over land and sea: over the land, it is parameterized through the friction velocity and the diffusivity characteristics of the gas and over the sea it is assumed to be small and only limited by the atmospheric resistance (Slinn and Slinn, 1980; Wesely, 1989; Draxler and Hess, 1997).  $v_g$  ( $\text{ms}^{-1}$ ), gravitational settling velocity for particles, is calculated as (Van der Hoven, 1968),

$$v_g = d_p^2 g (\rho_g - \rho) (18\mu)^{-1} \quad (2)$$

where  $d_p$  (m) is the particle diameter,  $g$  is the gravity of Earth ( $9.801 \text{ ms}^{-2}$ ),  $\rho$  ( $\text{gm}^{-3}$ ) is air density,  $\rho_g$  ( $\text{gm}^{-3}$ ) is particle density, and  $\mu$  is the dynamic viscosity of air ( $0.01789 \text{ gm}^{-1} \text{ s}^{-1}$ ). Note that  $v_g$  is zero for gases.

$R_c$  depends primarily upon a number of plant physiological and ground surface characteristics and is parameterized as (Wesely, 1989)

$$R_c = [1/(R_{st} + R_m) + 1/R_{cut} + 1/(R_{dc} + R_{cl}) + 1/(R_{ac} + R_g)]^{-1} \quad (3)$$

where  $R_{st}$  ( $\text{sm}^{-1}$ ) is the stomatal resistance,  $R_m$  ( $\text{sm}^{-1}$ ) is the mesophyll resistance,  $R_{cut}$  ( $\text{sm}^{-1}$ ) is the upper-canopy leaf cuticle (lu) resistance,  $R_{dc}$  is the resistance to gas-phase transfer by convection,  $R_{cl}$  ( $\text{sm}^{-1}$ ) is the lower canopy resistance,  $R_{ac}$  ( $\text{sm}^{-1}$ ) is the canopy height and density factor resistance, and  $R_g$  ( $\text{sm}^{-1}$ ) is the ground surface resistance.  $R_{st}$  is parameterized as

$$R_{st} = R_i D_{hx} [1 + (200/(G + 0.1))^2] [400/(T_s(40 - T_s))] \quad (4)$$

where  $R_i$  ( $\text{sm}^{-1}$ ) is the minimum resistance for water vapor, which depends upon season and land-cover,  $D_{hx}$  is the ratio of the diffusivity of water vapor to that of the pollutant,  $G$  ( $\text{Wm}^{-2}$ ) is the solar radiation reaching at the canopy, and  $T_s$  ( $^{\circ}\text{C}$ ) is the surface air temperature in the canopy. For temperatures outside the 0–40  $^{\circ}\text{C}$  temperature range,  $R_{st}$  is set to a very large value. The other resistances ( $R_m$ ,  $R_{cut}$ ,  $R_{dc}$ ,  $R_{cl}$ ,  $R_{ac}$ ,  $R_g$ ) depend primarily upon the effective (relative to  $\text{SO}_2$ ) Henry's constant and the specific reactivity of the pollutant. The parameterization of those resistances can be found in Draxler and Hess (1997).

### 2.2.2 Zhang dry deposition scheme

Another dry deposition scheme, based on the work of Zhang et al. (2001, 2003) (hereafter referred  
95 to as “ZDD”), has been added to STILT-Chem from version 0.7 as another option to calculate dry  
deposition of modeled gaseous and aerosol species (Wen et al., 2013). The ZDD scheme (Fig. 1)  
employs a methodology similar to the WDD scheme; however, it includes an improved represen-  
tation of a number of non-stomatal resistances, including in-canopy aerodynamic ( $R_{ac}$ ), soil ( $R_g$ ),  
and cuticle resistances ( $R_{cut}$ ). Instead of using a constant non-stomatal resistance for a particular  
100 season and land type, ZDD calculates non-stomatal resistance for two archetypal gas-phase species,  
 $SO_2$  and  $O_3$ , as a function of friction velocity, relative humidity, and canopy wetness, as well as  
biological factors, such as canopy type, leaf area index (LAI), and growing period. Non-stomatal  
resistances for other species are scaled as a weighted average to those of  $SO_2$  and  $O_3$  based on sim-  
ilarities or differences between their chemical and physical characteristics. Other improvements of  
105 the ZDD scheme include a more realistic treatment of cuticle and ground resistances in winter and  
the specification of seasonally-dependent input parameters, including LAI, roughness length, and  
resistance components (Zhang et al., 2003). The ZDD scheme, which is formulated for 26 land-use  
categories, can calculate dry deposition velocities for more than 30 gaseous species and 14 particu-  
late species that are usually considered in regional air quality models. It has been widely used in air  
110 quality models (e.g., Zhang et al., 2002; Alexander et al., 2005; Nopmongcol et al., 2012).

### 2.3 Bi-directional $NH_3$ air-surface exchange scheme

In order to simulate bi-directional exchange of  $NH_3$  between the atmosphere and the Earth’s surface,  
a bi-directional air-surface exchange scheme developed by Zhang et al. (2010) (hereafter referred to  
as “ZBE”) was implemented into STILT-Chem v0.8 in this study. The ZBE scheme (see Fig. 1) was  
115 developed for application in region-scale air quality models, in which stomatal and soil emission  
potentials are specified according to land-use category and season based on an extensive review of  
measurement and model studies.

In this scheme, the overall vertical flux  $F_t$  ( $\mu g m^{-2} s^{-1}$ ) at a reference height above the canopy  
can be calculated as

$$F_t = -\frac{(\chi_a - \chi_c)}{(R_a + R_b)} \quad (5)$$

where  $\chi_a$  ( $\mu g m^{-3}$ ) is the  $NH_3$  air concentration at the reference height, and  $\chi_c$  ( $\mu g m^{-3}$ ) is the  $NH_3$

air concentration at the canopy top and can be calculated as

$$\chi_c = \left( \frac{\chi_a}{R_a + R_b} + \frac{\chi_{st}}{R_{st} + R_m} + \frac{\chi_g}{R_{ac} + R_g} \right) \cdot \left( \frac{1}{R_a + R_b} + \frac{1}{R_{st} + R_m} + \frac{1}{R_{ac} + R_g} + \frac{1}{R_{cut}} \right)^{-1} \quad (6)$$

where  $\chi_{st}$  ( $\mu\text{g m}^{-3}$ ) is the stomatal compensation point and  $\chi_g$  ( $\mu\text{g m}^{-3}$ ) is the soil compensation point. The same formulas used in the ZDD scheme are used in the ZBE scheme to calculate all of the resistances in Eq. (6). All of those formulas can be found in the work of Zhang et al. (2003).

$\chi_{st}$  is defined chemically as the concentration at which there is both a thermodynamic equilibrium between  $\text{NH}_3$  in the liquid and gas phases and an acid-base equilibrium between  $\text{NH}_4^+$  and  $\text{NH}_3$  in the liquid phase.  $\chi_{st}$  can be either measured or calculated according to the formula (Nemitz et al., 2004)

$$\chi_{st} = 1.703 \times 10^{10} \left( \frac{161500}{T_{st}} \right) \exp \left( -\frac{10378}{T_{st}} \right) \Gamma_{st} \quad (7)$$

where  $T_{st}$  (K) is the temperature of the leaf stomata, and  $\Gamma_{st}$  is the stomatal emission potential at 1 atmosphere and is given by the expression (Nemitz et al., 2000)

$$\Gamma_{st} = \frac{[\text{NH}_4^+]_{st}}{[\text{H}^+]_{st}} \quad (8)$$

where  $[\text{NH}_4^+]_{st}$  is the concentration of  $\text{NH}_4^+$  ( $\text{mol L}^{-1}$ ) in the apoplastic fluid (fluid in a tissue-level compartment formed by the continuum of cell walls of adjacent cells as well as the extracellular spaces).  $[\text{H}^+]_{st} = 10^{-\text{pH}}$  is the stomatal concentration of  $\text{H}^+$  ( $\text{mol L}^{-1}$ ) with the pH of the intercellular fluid at 1 atmosphere.

Similarly,  $\chi_g$  is calculated (Nemitz et al., 2004) using the formulas

$$\chi_g = 1.703 \times 10^{10} \left( \frac{161500}{T_g} \right) \exp \left( -\frac{10378}{T_g} \right) \Gamma_g \quad (9)$$

$$\Gamma_g = \frac{[\text{NH}_4^+]_g}{[\text{H}^+]_g} \quad (10)$$

where  $T_g$  (K) is the temperature of the ground surface,  $\Gamma_{st}$  is the stomatal emission potential, and  $[\text{NH}_4^+]_g$  and  $[\text{H}^+]_g$  are the concentrations of  $\text{NH}_4^+$  and  $\text{H}^+$  ( $\text{mol L}^{-1}$ ) in the ground cover.

In the ZBE scheme, a set of stomatal ( $\Gamma_{st}$ ) and ground ( $\Gamma_g$ ) emission potentials are specified (Table 1) as inputs for each land-use category using empirically-derived values to generate  $\chi_{st}$  and  $\chi_g$  using Eqs. (7) and (9), respectively. This approach is especially useful for regional-scale air quality models because emission-potential values are generally not measured at regional scales and are not explicitly calculated in regional-scale models. These values are based on an extensive review of

model and measurement studies. As a result, they are generally representative of emission potentials for each land-use category and season. For forests and grasslands, two sets of  $\Gamma_{st}$  and  $\Gamma_g$  values are provided for the same land-use category to reflect different nitrogen contents – one for high-N canopies and the other for low-N canopies. For the atmospheric  $\text{NH}_3$  modeling studies in which anthropogenic  $\text{NH}_3$  emissions are used as an external input, following Eq. (6) the air concentration of  $\text{NH}_3$  at the canopy top  $\chi_c$  can be calculated as (Trebs et al., 2006)

$$\chi_c = \left( \frac{\chi_a}{R_a + R_b} + \frac{\chi_{st}}{R_{st} + R_m} + \frac{\chi_g}{R_{ac} + R_g} + F_e \right) \cdot \left( \frac{1}{R_a + R_b} + \frac{1}{R_{st} + R_m} + \frac{1}{R_{ac} + R_g} + \frac{1}{R_{cut}} \right)^{-1} \quad (11)$$

where  $F_e$  ( $\mu\text{g m}^{-2} \text{s}^{-1}$ ) is the  $\text{NH}_3$  anthropogenic emission flux from external inputs.

### 3 Model simulations

#### 3.1 Measurements used for simulation and comparison

130 Detailed measurements of surface  $\text{NH}_3$  concentrations were carried out during the Southern Ontario  
 Ammonia Passive Sampler Survey (SOAPSS), which ran from 4 April 2006 to 27 March 2007 (Vet  
 et al., 2008). The objective of SOAPSS was to measure ambient concentrations of  $\text{NH}_3$  at approx-  
 imately 79 sites, mainly located in southern Ontario but also at a small number of Canadian sites  
 outside of Ontario and US sites bordering the Great Lakes. The survey provided highly spatially-  
 135 resolved atmospheric  $\text{NH}_3$  concentration data, with distances between sites in southern Ontario of  
 approximately 20 km. The  $\text{NH}_3$  measurements were made using passive samplers and represent an  
 integrated average of the near-surface  $\text{NH}_3$  concentration over a one-week (before December 2006)  
 or two-week (after November 2006) period. Out of all sites, 53 were selected as receptors and  
 test sites in this study (Fig. 2), consisting of 39 agricultural sites and 14 forest sites. The other 26  
 140 sites, which were very close to transitions from one land-use type to another, were not used in this  
 study because their land-use types cannot be assigned with certainty at the model grid scale due to  
 insufficient resolution of the meteorological input.

#### 3.2 Simulation setup

STILT-Chem v0.8 was used to simulate hourly  $\text{NH}_3$  concentrations at the 53 sites (Fig. 2) for a pe-  
 145 riod from 1 June to 30 November 2006. The model was driven by Eta Data Assimilation System  
 (EDAS) data that were obtained from NOAA's Air Resources Laboratory (ARL) meteorological  
 data archives. The EDAS data cover most of North America using  $185 \times 129$  grid cells with a hor-  
 izontal spacing of 40 km. The EDAS data consists of 26 vertical layers with a model top of 25 mb  
 and are available at 3 hourly intervals. In the model simulations, ensembles of 500 particles were

150 released every hour from each receptor site location at a height of 5 m above ground. A particle  
ensemble size of 500 was shown in a previous study (Wen et al., 2013), using the same model and  
similar inputs, to be sufficient to achieve adequate accuracy while not considerably increasing the  
computational cost. The paths of the particles were followed backward in time for six days, which  
usually allowed them to travel far away from any sources near the receptors. The calculated back-  
155 trajectories were 3-dimensional and their vertical motions were calculated directly using vertical  
velocity fields provided in the input meteorological data. The size of the integration time steps for  
the back-trajectory calculations varied with time and location from 1 min to 1 h and was computed  
based on the requirement that the advection distance per time-step should be less than the grid spac-  
ing (Courant–Friedrichs–Lewy condition). The same time steps were then also used in the forward  
160 simulation for deposition and chemistry calculations.

Identical emissions and initial/boundary conditions to those described in Wen et al. (2013) were  
employed in this study. A detailed description of the emissions and initial/boundary conditions can  
be found in Wen et al. (2013), but a brief summary is provided here. Concentrations of modeled  
species were initialized at the endpoints of trajectories using output from the Model for Ozone And  
165 Related chemical Tracers, version 4 (MOZART-4) (Emmons et al., 2010), which was obtained from  
the WRF-Chem website (<http://www.acd.ucar.edu/wrf-chem/mozart.shtml>). The gridded MOZART-  
4 output fields have a  $2.8^\circ \times 2.8^\circ$  horizontal grid spacing with 28 vertical levels from the surface to  
approximately 2 hPa in six-hourly intervals. No interpolation of the output was performed for the  
particle concentration initialization. MOZART-4 chemical species were mapped onto CB4 species  
170 according to the matching table given by Emmons et al. (2010). The initial concentrations of par-  
ticles at trajectory endpoints were then evolved forward in time to account for the influences of  
emissions, chemical reactions and deposition along each trajectory for each time step in the forward  
trajectory integrations.

The 2006 Canadian Criteria Air Contaminants emission inventory (version 2) from Environment  
175 Canada (EC) was employed as the Canadian emission inventory in the simulations, which incorpo-  
rates facility-level emissions from the EC National Pollutant Release Inventory (i.e., point sources)  
plus province-level estimates of on-road mobile emissions, off-road mobile emissions, and area  
emissions (<http://www.ec.gc.ca/inrp-npri/>). A special inventory of 2006 Canadian agricultural  $\text{NH}_3$   
emissions that was developed under the Canadian National Agri-Environmental Standards Initiative  
180 (NAESI) was also included (Makar et al., 2009) to represent regional differences in farming prac-  
tices and climatic conditions for each livestock category, and temporal variation due to seasonally  
varying agricultural practices or temperatures. The corresponding US and Mexican emissions in-  
ventories that were used were the 2005 US National Emissions Inventory (version 4) and the 1999  
Mexican emissions inventory. Both were obtained from the US Environmental Protection Agency  
185 (<http://www.epa.gov/ttn/chief/eiinformation.html>). These three national anthropogenic inventories  
all included emissions of oxides of nitrogen ( $\text{NO}_x$ ), volatile organic compounds (VOC),  $\text{NH}_3$ , car-

bon monoxide (CO), oxides of sulphur (SO<sub>x</sub>), and primary particulate matter (PM) with an aerodynamic diameter less than or equal to 10 μm and 2.5 μm (PM<sub>10</sub> and PM<sub>2.5</sub>). Each of the three national emissions inventories was processed with the Sparse Matrix Operator Kernel Emission (SMOKE) (v2.4) (UNC, 2009) emissions processing system for a domain (Fig. 2) that consisted of 150 × 106 grid cells with a horizontal grid spacing of 42 km on a secant-polar-stereographic map projection true at 60° N. The SMOKE-processed output emissions consisted of hourly gridded emissions fields that accounted for geographic variations and diurnal, weekly and monthly variations. For simplicity all point sources were treated as surface sources, which is reasonable for NH<sub>3</sub> emissions because all point sources together account for only a small fraction of total NH<sub>3</sub> emission ([http://www.ec.gc.ca/inrp-npri/default.asp?lang=en&n=0EC58C98-1#Emission\\_Summaries](http://www.ec.gc.ca/inrp-npri/default.asp?lang=en&n=0EC58C98-1#Emission_Summaries)).

Three dry deposition schemes, including two uni-directional schemes – ZDD and WDD – and the bi-directional scheme ZBE, were used in different STILT-Chem simulations for the 1 June to 30 November 2006 period to investigate their impacts on model predictions of NH<sub>3</sub> ambient concentrations. In the ZBE scheme, as mentioned above (Sect. 2.3), two sets of  $\Gamma_{st}$  and  $\Gamma_g$  values are available for the same land-use category for forests and grasslands according to canopy nitrogen content. Zhang et al. (2010) suggested that the higher values should be chosen for high-N canopies and the lower values should be chosen for low-N canopies. The classification of high-N and low-N canopy for each model grid cell can be determined according to a total nitrogen deposition map for the model domain obtained either from measurements or previous mode runs. In this study, due to a lack of such N deposition maps, we assumed low-N canopies for all forests and grasslands. This assumption appears to be reasonable because forest areas near the southern Ontario test sites have low NH<sub>3</sub> emission strengths and concentrations (cf. Figs. 2 and 3); thus N deposition in those forest areas should be low because NH<sub>3</sub> tends to be a local pollutant. Accordingly, in the STILT-Chem simulation with the ZBE scheme, the minimum emission potential values listed in Table 1 were used and the simulation was treated as a base-case simulation. However, the difference in the modeled NH<sub>3</sub> concentrations between simulations by assuming low-N canopies and by assuming high-N canopies for all forests and grasslands was examined. Some sensitivity simulations were also performed in which larger emission potential values were used for agricultural land-use categories in the ZBE scheme (see Sect. 4.3).

## 4 Results

### 4.1 Measured and modeled NH<sub>3</sub> concentrations using different dry deposition schemes

Figure 3 shows a site-by-site comparison of average NH<sub>3</sub> concentrations between simulations and observations, in which hourly modeled and weekly observed NH<sub>3</sub> concentrations were averaged over the entire simulation period from 1 June to 30 November 2006 for each receptor site for the three simulations that used each of the three deposition schemes. Based on the good agreement

obtained between simulated and observed values for a similar simulation (Wen et al., 2013), we assumed that the NH<sub>3</sub> emission inventory used in this study is reasonable and that the modeled physical and chemical processes (other than dry deposition schemes) do not bias NH<sub>3</sub> concentration systematically over the regional scale, so that differences in the modeled NH<sub>3</sub> concentration from using the three dry deposition schemes can be compared. Note again that the minimum values of stomatal emission potentials and ground emission potentials given in Table 1 were used in the simulation using the ZBE scheme. We can see from Fig. 3 that the STILT-Chem model using all three schemes generally performed adequately in predicting the average levels of observations for most sites, and also performed well in capturing the general transitional trend in the observations going from forested regions to agricultural regions (see Fig. 2). This is a positive result considering the fact that NH<sub>3</sub> is generally difficult for air quality models to simulate due to its strong spatial variability. Although STILT-Chem is based on a Lagrangian reference framework and is capable of capturing sub-grid-scale variability (Wen et al., 2011), some processes such as emissions are associated with Eulerian grids in the simulation, and thus the model's performance is still affected by the spatial resolution of input fields. Overall, out of the three schemes, NH<sub>3</sub> concentrations predicted using the ZDD scheme were smallest mainly because this scheme generally gives higher NH<sub>3</sub> dry deposition velocities (see Sect. 4.2). The highest NH<sub>3</sub> concentrations were predicted by the ZBE scheme due mainly to the inclusion of additional NH<sub>3</sub> emissions from ground and canopy vegetation.

Figure 4a shows correlations between observed and modeled mean NH<sub>3</sub> concentrations that are presented in Fig. 3 for the three schemes. The ZBE scheme generally predicted higher NH<sub>3</sub> concentration averages over the entire simulation period than the ZDD and WDD schemes. However, all three schemes produced almost equivalent correlation patterns with the observations. They underestimated NH<sub>3</sub> concentrations at sites with high observed concentrations, while overestimating NH<sub>3</sub> concentrations at sites with low observed concentrations. This phenomenon is more evident in the scatter plots (Figs. 4b, c and d) in which weekly measured and modeled concentrations were used. Similar results have been reported by a European study that used the LOTOS-EUROS model (Wichink Kruit et al., 2012), in which NH<sub>3</sub> concentrations in natural areas were slightly overestimated, whereas NH<sub>3</sub> concentrations in agricultural regions were underestimated, with more pronounced underestimations as observed NH<sub>3</sub> levels increased. In terms of statistical values of the Ratio Of the Means (ROM) and the Mean Fractional Bias (MFB) (Tables 2 and 3), modeled NH<sub>3</sub> concentrations at agricultural sites were overall underestimated by WDD and ZDD in this study, and slightly overestimated by ZBE, but all three schemes significantly underestimated NH<sub>3</sub> concentrations for sites with observed levels greater than 6.0 µg m<sup>-3</sup>, with a tendency to underestimate more with increasing observed concentrations (Fig. 4). The performances of the three schemes at agricultural sites were not obviously different according to their correlations with observations but differed significantly from the perspective of bias (Fig. 4 and Table 3). All three schemes performed

poorly in reproducing observed concentrations at the forest sites, with considerable overestimation  
260 and ineffective representation of the pattern of observations, probably due to much lower emissions  
strengths and concentration levels at those sites. The same uncertainty in the simulations may lead to  
more pronounced error/bias at low concentrations than high concentrations. According to the values  
of ROM, MFB and Mean Fractional Error (MFE) in Table 3, the ZBE scheme performed the best for  
agricultural sites and for all sites, whereas the ZDD scheme had the best performance in simulating  
265  $\text{NH}_3$  concentrations for the forested sites.

Figure 5 shows time series of observed and simulated  $\text{NH}_3$  concentrations, in which modeled  
hourly  $\text{NH}_3$  concentrations were averaged according to corresponding weekly sampling periods,  
and then observed and modeled weekly concentrations were averaged over receptor sites for three  
groups: forest sites, agricultural sites, and all sites. All three schemes generally performed well  
270 in capturing the timing of peaks in the observations, albeit the exact predicted concentration levels  
were different. From statistics calculated using values of the mean time series displayed in Fig. 5,  
the ZDD scheme performed best in capturing average levels of observation for forest sites, with a  
ROM of 0.95, compared with 1.27 for WDD and 1.68 for ZBE, respectively. The ZBE scheme, on  
the other hand, performed best in capturing average levels for both agricultural sites and all sites.  
275 For agricultural sites ZBE had a ROM of 1.04, compared 0.73 for ZDD and 0.83 for WDD, and  
for all sites the ZBE scheme had a ROM of 1.07, compared with 0.74 for ZDD and 0.85 for WDD.  
All three schemes had relatively poor correlations with observations for all three groups of sites,  
with a maximum value of 0.48. The ZBE scheme substantially overestimated  $\text{NH}_3$  concentrations  
over forest sites and the ZDD scheme obviously underestimated  $\text{NH}_3$  concentrations over agricul-  
280 tural sites. Their performances also differed for different simulation periods. Before mid-October,  
both WDD and ZDD can predict  $\text{NH}_3$  concentrations well, indicating that the anthropogenic  $\text{NH}_3$   
emissions used for this period of time were reasonable. After mid-October, however, there was a  
universal sharp decrease in modeled  $\text{NH}_3$  concentrations (especially at agricultural sites), mainly in  
response to a reduction of the estimated  $\text{NH}_3$  emissions as a result of lower emissions of  $\text{NH}_3$  from  
285 livestock production and fertilizer application in southern Ontario in the winter months (Lillyman  
et al., 2010), as well as by the presence of snow cover, which typically begins in November in south-  
ern Ontario and which can substantially reduce  $\text{NH}_3$  soil emissions. However, the big difference  
between modeled and observed  $\text{NH}_3$  concentrations for all three schemes after mid-October may  
suggest a significant underestimation of anthropogenic  $\text{NH}_3$  emissions after mid-October, presum-  
290 ably as a result of neglecting likely fertilizer application from October to November in preparation  
for the next year's agricultural activity. As for the period before mid-August, the two uni-direction  
schemes predicted  $\text{NH}_3$  well whereas ZBE obviously overestimated. The overestimation of ZBE  
was probably due to the use of constant stomatal emission potentials for the entire modeling period,  
which are likely too high for this period of time. By contrast the modeled results by ZBE agree  
295 well with the observations at the forest sites after mid-October and at the agricultural sites from

mid-August to mid-October. Since temperature generally decreases after mid-August and  $\text{NH}_3$  concentrations overall were overestimated before mid-August, the good agreement later on could be a result of lower temperatures because stomatal and ground compensation points decrease exponentially with decreasing temperature (Eqs. 7 and 9).

## 300 4.2 Modeled dry deposition velocity and flux using different schemes

Hourly modeled results for the entire simulation period were used to calculate average diurnal variations of  $\text{NH}_3$  concentration, dry deposition velocity and air/surface exchange flux. The resulting average diurnal variations in these three quantities for the three schemes are presented in Fig. 6 for the forest sites and the agricultural sites. Figure 6 shows that the dry deposition velocities of  $\text{NH}_3$  modeled by the WDD scheme were smaller than those modeled by the ZDD scheme for both the agricultural and especially for the forest sites. The underestimation of dry deposition velocities by the WDD scheme has been reported by other studies (Wu et al., 2012) and was attributed to the use of a prescribed minimum non-stomatal resistance without consideration of key biological factors (e.g., LAI). In contrast, the non-stomatal resistance parameterizations adopted in the ZDD scheme vary with biological (LAI), meteorological (friction velocity, relative humidity), and surface (canopy wetness) conditions, and therefore are better able to capture the variations of dry deposition velocity than the simple non-stomatal resistance parameterization in the WDD scheme. The  $\text{NH}_3$  dry deposition velocity estimated by WDD for forest sites was even smaller than that for the agricultural sites, mainly due to the exclusion of stomatal uptake (through the use of a very large value of  $10^{25} \text{ s m}^{-1}$  for minimum canopy stomatal resistance) for the deciduous forest category in the “autumn” season. In WDD, September–October is treated as autumn and foliage loss is thus assumed. The underprediction of dry deposition velocities of  $\text{O}_3$  by the WDD scheme for September – October has also been reported (Wu et al., 2011). The ZBE scheme, on the other hand, calculated  $\text{NH}_3$  flux directly and no  $\text{NH}_3$  dry deposition velocity was estimated in the ZBE scheme. In order to compare with the other schemes, we divided  $\text{NH}_3$  fluxes by corresponding  $\text{NH}_3$  concentrations to obtain an “effective” dry deposition velocity for the ZBE scheme. Hence diurnal patterns of effective dry deposition for the ZBE scheme are presented in Fig. 6 as well. The effective dry deposition velocities from the ZBE scheme clearly show strong  $\text{NH}_3$  emission (negative values) from surface to the atmosphere during the daytime for both forest and agricultural sites. During the nighttime, ZBE effective deposition velocities are close to the dry deposition velocities estimated by ZDD for forest sites, but they are small and negative for agricultural sites.

Modeled  $\text{NH}_3$  fluxes using ZDD and WDD show evident diurnal patterns in which magnitude of fluxes were smaller at night and larger during daytime hours. All fluxes were negative (downward out of the atmosphere) due to consideration solely of dry deposition in those uni-directional schemes. Although modeled  $\text{NH}_3$  dry deposition velocities by ZDD were larger for forest sites than for agricultural sites,  $\text{NH}_3$  fluxes modeled by both WDD and ZDD were higher for agricultural sites

than for forest sites. The main reason is that dry deposition flux is determined not only by dry deposition velocity but also by ambient concentration, and  $\text{NH}_3$  concentrations at the agricultural sites were much higher than those at the forest sites as shown in the top panel of Fig. 6. Downward fluxes predicted by ZDD were greater than those predicted by WDD for both forest and agricultural sites: as a consequence, modeled  $\text{NH}_3$  concentrations based on ZDD were generally smaller than those based on WDD (see also Figs. 3 and 5).

Unlike the diurnal patterns of  $\text{NH}_3$  surface fluxes predicted by the uni-directional schemes, in which all fluxes were downward (negative), the  $\text{NH}_3$  surface fluxes predicted by the ZBE scheme were mostly upward (positive), especially for the agricultural sites where almost all fluxes were positive and had a much higher peak. Estimated fluxes over the forest sites were negative at night (Fig. 6) but reached maximum (positive) values in the afternoon. Flux peaks for both the agricultural sites and the forest sites are coincident with the ambient concentration minima as expected from Eq. (5). The mean flux of the diurnal pattern was about  $-1.2 \text{ ngm}^{-2}\text{s}^{-1}$  for the forest sites, and  $19.2 \text{ ngm}^{-2}\text{s}^{-1}$  for the agricultural sites, indicating that  $\text{NH}_3$  air/surface exchange at the agricultural sites acted as an important source of  $\text{NH}_3$  to the atmosphere during the study period, based on the ZBE results.

### 4.3 Uncertainty associated with emission potentials in the ZBE scheme

As discussed in Sect. 2.3, two parameters are required to determine air/surface exchange of  $\text{NH}_3$ : stomatal emission potential ( $\Gamma_{\text{st}}$ ) and soil emission potential ( $\Gamma_{\text{g}}$ ). Although these parameters can be measured at selected locations, they are not available at regional scales nor are they calculated in regional-scale air quality models. For regional-scale air quality modeling applications, the ZBE scheme employs  $\Gamma_{\text{st}}$  and  $\Gamma_{\text{g}}$  values that have been derived empirically for each land-use category. Two empirical sets of  $\Gamma_{\text{st}}$  and  $\Gamma_{\text{g}}$  values were provided (Table 1) to reflect different nitrogen contents for the same land-use category that forests and grasslands might have. Thus the use of different empirical emission potential values could lead to different simulation results.

In order to bracket uncertainties in modeled  $\text{NH}_3$  concentrations associated with the use of the different emission-potential values, we ran the model twice – once using the minimum and again using the maximum emission potentials given in Table 1 – with the ZBE scheme for every location in the simulation domain. Note that for some land-use categories (e.g., crops) the same emission potential was used for both runs due to only one value being available. Modeled  $\text{NH}_3$  concentrations were then averaged over the entire simulation period for each test site, and the average concentrations for the two runs are presented in Fig. 7 for comparison. Figure 7 shows that differences in modeled  $\text{NH}_3$  concentrations from using the maximum and minimum emission potentials were marked, especially for most forest sites. Using maximum emission potentials not only greatly overestimated  $\text{NH}_3$  concentrations, but also significantly reduced the correlation between simulation and observations. The mean  $\text{NH}_3$  concentration for the forest sites was  $2.25 \text{ }\mu\text{gm}^{-3}$  when maximum emission potentials

were used, about four times the mean value of  $0.54 \mu\text{g m}^{-3}$  obtained when the minimum emission potentials were used. This result indicates the importance of using appropriate emission potentials in  
370  $\text{NH}_3$  bi-directional modeling. Although the same emission potential values were used for both runs for agricultural locations (agriculture related land-use categories only had one emission-potential value: see Table 1), differences in modeled concentrations for those locations were still evident. The mean  $\text{NH}_3$  concentration for agricultural sites was  $3.81 \mu\text{g m}^{-3}$  when maximum emission potentials were used, approximately 1.5 times the mean concentration of  $2.42 \mu\text{g m}^{-3}$  obtained using minimum  
375 emission potentials. This difference resulted from the transport of higher  $\text{NH}_3$  concentrations from forest areas when maximum emission potentials were used.

Figure 8 shows relationships between deviations of modeled  $\text{NH}_3$  concentrations from observations and corresponding local mean anthropogenic  $\text{NH}_3$  emissions for each site (see Fig. 2). All data points in Fig. 8 are means over the entire simulation period for the 53 sites for all three schemes.  
380 Those for the ZBE scheme were the outcome of using minimum emission potentials. The deviations of modeled  $\text{NH}_3$  concentrations from observed values obviously show a negative correlation with anthropogenic  $\text{NH}_3$  emissions, which is more obvious for ZBE than for the other schemes. When anthropogenic emissions strength was greater than  $6.0 \text{ mole s}^{-1} \text{ gridcell}^{-1}$ , all three schemes underestimated  $\text{NH}_3$  concentrations. Even for the ZBE scheme which generally predicts the highest  
385 concentrations among the schemes, the underestimation can still be significant. The underestimation of  $\text{NH}_3$  concentrations indicates that emission potentials specified in the ZBE scheme (Table 1) might be not large enough for those highly polluted sites.

In order to quantify how much emission potentials might potentially be underestimated, we conducted several sensitivity tests using different emission potentials for all locations where mean anthropogenic  $\text{NH}_3$  emissions exceeded  $6.0 \text{ mole s}^{-1} \text{ gridcell}^{-1}$ . Out of 53 sites, there were five agricultural sites that satisfied this condition. Those five sites were selected as test sites in this sensitivity study. The values of emission potentials tested were 2, 3, 4, and 6 times the magnitudes of the pre-defined values in Table 1 for land-use categories related to agriculture (categories 15 to 20 in Table 1). Note that those categories only have one emission-potential value for each category. Modeled mean  
395  $\text{NH}_3$  concentrations over the entire simulation period were compared for these tests with observations and results are summarized in Table 4. Examination of Table 4 suggests that there is a strong sensitivity to the choice of emission potential value. It further suggests that the pre-defined values of the emission potentials used in the ZBE scheme might be substantially underestimated for sites with strong anthropogenic  $\text{NH}_3$  emissions. According to these tests, values of emission potentials at least  
400 three times larger than those specified in Table 1 are required in order to reasonably predict  $\text{NH}_3$  concentrations at sites with anthropogenic emission strengths greater than  $6.0 \text{ mole s}^{-1} \text{ gridcell}^{-1}$ .

## 5 Summary and conclusions

An air/surface bi-directional exchange scheme developed for regional  $\text{NH}_3$  modeling was incorporated in the STILT-Chem v0.8 air quality model for this study. STILT-Chem v0.8 was then applied  
405 to simulate  $\text{NH}_3$  concentration at 53 measurement sites in southern Ontario for a simulation period from 1 June to 30 November 2006, using the bi-directional scheme (ZBE) and two uni-directional dry deposition schemes (WDD and ZDD). Modeled  $\text{NH}_3$  concentrations obtained using these three schemes were compared against weekly passive-sampler  $\text{NH}_3$  measurements for each site. The comparisons indicate that in general all three schemes can reproduce the observed  $\text{NH}_3$  concentra-  
410 tions reasonably well. However, the three schemes performed differently at locations with different  $\text{NH}_3$  concentration levels. Modeled results show that the bi-directional scheme performed best at locations with high observed  $\text{NH}_3$  concentrations but overestimated  $\text{NH}_3$  levels for locations with low observed  $\text{NH}_3$  concentrations. The two uni-directional dry deposition schemes, on the other hand, generally performed better than the bi-directional scheme at sites with low observed  $\text{NH}_3$   
415 concentrations.

The absolute or relative errors in the modeled  $\text{NH}_3$  concentrations obtained using the three different dry deposition schemes were examined and interpreted based on the assumption that other processes did not cause any systematic biases. One possible systematic bias, however, could be caused by the underestimation of  $\text{NH}_3$  emissions, as emissions data for biogeochemical sources like  
420 biogenic N fixation in agricultural systems and/or atmospheric deposition of  $\text{NO}_y$  followed by soil N cycling processes (e.g., Beusen et al., 2008; Galloway et al., 2008) are generally not available and hence are not included in available  $\text{NH}_3$  emissions inventories. The omission of such emissions could lead to underestimation of atmospheric  $\text{NH}_3$  concentrations. Although the appropriateness of this assumption could not be verified directly in this study, the good agreement between model  
425 simulations and observations suggests that systematic biases in the simulations are small. Moreover, the absolute or relative errors caused by those systematic biases might be shifted to one direction only because the same model and input data were used for all three dry deposition schemes.

If stomatal and ground emission potentials were set to zero in the ZBE scheme, the ZBE scheme and the ZDD scheme would yield the same  $\text{NH}_3$  flux. The reason is that the ZBE scheme was devel-  
430 oped from the ZDD scheme and both schemes uses the same formulas to compute the dry deposition component (Zhang et al., 2010). In other words, the ZDD scheme acts as a special case of the ZBE scheme in  $\text{NH}_3$  bi-directional exchange modeling. Since the ZDD scheme more accurately predicted  $\text{NH}_3$  concentrations at locations with low  $\text{NH}_3$  concentrations than the ZBE scheme (Fig. 4), the appropriateness of the application of the current version of the bi-directional scheme to low  $\text{NH}_3$   
435 concentration locations needs reconsideration and further investigation. Uncertainties in the magnitudes of the emission-potential values used for both low-  $\text{NH}_3$  and high- $\text{NH}_3$  concentration locations also require more research.

## 6 Code availability

STILT-Chem v0.8 is written in Fortran. Model runs are controlled by a shell script. A brief manual  
440 is included in the model package. The STILT-Chem v0.8 model code will be available online for  
free access in the near future. For the time being, the model can be obtained by contacting John C.  
Lin (john.lin@utah.edu).

*Acknowledgements.* We gratefully acknowledge funding from Environment Canada for supporting D. Wen and  
the important contribution of G. Beaney of Environment Canada in making the SOAPSS ammonia measure-  
445 ments. We also thank Q. Zheng and J. Zhang of Environment Canada for preparing the emissions files used  
in this study. This work was made possible by the facilities of the Shared Hierarchical Academic Research  
Computing Network (SHARCNET: <http://www.sharcnet.ca>) and Compute/Calcul Canada.

## References

- Alexander, B., Park, R. J., Jacob, D. J., Li, Q. B., Yantosca, R. M., Savarino, J., Lee, C. C. W., and  
450 Thiemens, M. H.: Sulfate formation in sea-salt aerosols: constraints from oxygen isotopes, *J. Geophys. Res.*, 110, D10307, doi:10.1029/2004JD005659, 2005.
- Bash, J. O., Cooter, E. J., Dennis, R. L., Walker, J. T., and Pleim, J. E.: Evaluation of a regional air-quality model with bidirectional  $\text{NH}_3$  exchange coupled to an agroecosystem model, *Biogeosciences*, 10, 1635–1645, doi:10.5194/bg-10-1635-2013, 2013.
- 455 Beusen, A., Bouwman, A. F., Heuberger, P., Van Drecht, G., and Van Der Hoek, K. W.: Bottomup uncertainty estimates of global ammonia emissions from global agricultural production systems, *Atmos. Environ.*, 42, 6067–6077, doi:10.1016/j.atmosenv.2008.03.044, 2008.
- Chang, J. S.: NAPAP Report 4, the regional acid deposition model and engineering model, Appendix E, in: *Acid Deposition: State of Science and Technology*, vol I, Emissions, Atmospheric Processes, and Deposition, US  
460 Government Printing Office, Washington, DC, 20402–9325, 1990.
- Cooter, E. J., Bash, J. O., Walker, J. T., Jones, M. R., and Robarge, W.: Estimation of  $\text{NH}_3$  bi-directional flux from managed agricultural soils, *Atmos. Environ.*, 44, 2107–2115, doi:10.1016/j.atmosenv.2010.02.044, 2010.
- Cooter, E. J., Bash, J. O., Benson, V., and Ran, L.: Linking agricultural crop management and air quality models  
465 for regional to national-scale nitrogen assessments, *Biogeosciences*, 9, 4023–4035, doi:10.5194/bg-9-4023-2012, 2012.
- Draxler, R. R. and Hess, G. D.: Description of the HYSPLIT 4 Modeling System, NOAA Technical Memorandum ERL ARL-224, 1997.
- Emmons, L. K., Walters, S., Hess, P. G., Lamarque, J.-F., Pfister, G. G., Fillmore, D., Granier, C., Guenther, A., Kinnison, D., Laepple, T., Orlando, J., Tie, X., Tyndall, G., Wiedinmyer, C., Baughcum, S. L., and  
470 Kloster, S.: Description and evaluation of the Model for Ozone and Related chemical Tracers, version 4 (MOZART-4), *Geosci. Model Dev.*, 3, 43–67, doi:10.5194/gmd-3-43-2010, 2010.
- Flechard, C. R., Massad, R.-S., Loubet, B., Personne, E., Simpson, D., Bash, J. O., Cooter, E. J., Nemitz, E., and Sutton, M. A.: Advances in understanding, models and parameterizations of biosphere-atmosphere ammonia  
475 exchange, *Biogeosciences*, 10, 5183–5225, doi:10.5194/bg-10-5183-2013, 2013.
- Galloway, J. N., Townsend, A. R., Erisman, J. W., Bekunda, M., Cai, Z., Freney, J. R., Martinelli, L. A., Seitzinger, S. P., and Sutton, M. A.: Transformation of the nitrogen cycle: recent trends, questions, and potential solutions, *Science*, 320, 889–892, doi:10.1126/science.1136674, 2008.
- Geels, C., Andersen, H. V., Ambelas Skjøth, C., Christensen, J. H., Ellermann, T., Løfstrøm, P.,  
480 Gyldenkerne, S., Brandt, J., Hansen, K. M., Frohn, L. M., and Hertel, O.: Improved modelling of atmospheric ammonia over Denmark using the coupled modelling system DAMOS, *Biogeosciences*, 9, 2625–2647, doi:10.5194/bg-9-2625-2012, 2012.
- Gery, M. W., Whitten, G. Z., Killus, J. P., and Dodge, M. C.: A photochemical kinetics mechanism for urban and regional scale computer modeling, *J. Geophys. Res.*, 94, 12925–12956, doi:10.1029/JD094iD10p12925,  
485 1989.
- Lillyman, C., Buset, K., and Mullins, D.: 2008 Canadian Atmospheric Assessment of Agricultural Ammonia, National Agri-Environmental Standards, Environment Canada, Gatineau, Que, ISBN 9781100124209, 295

pp., 2010.

- 490 Lin, J. C., Gerbig, C., Wofsy, S. C., Andrews, A. E., Daube, B. C., Davis, K. J., and Grainger, C. A.: A near-field tool for simulating the upstream influence of atmospheric observations: the Stochastic Time-inverted Lagrangian Transport (STILT) model, *J. Geophys. Res.*, 108, 4493, doi:10.1029/2002JD003161, 2003.
- Makar, P. A., Moran, M. D., Zheng, Q., Cousineau, S., Sassi, M., Duhamel, A., Besner, M., Davignon, D., Crevier, L.-P., and Bouchet, V. S.: Modelling the impacts of ammonia emissions reductions on North American air quality, *Atmos. Chem. Phys.*, 9, 7183–7212, doi:10.5194/acp-9-7183-2009, 2009.
- 495 Morris, J. T.: Effects of nitrogen loading on wetland ecosystems with particular reference to atmospheric deposition, *Annu. Rev. Ecol. Syst.*, 22, 257–279, doi:10.1146/annurev.es.22.110191.001353, 1991.
- Nemitz, E., Sutton, M. A., Schjoerring, J. K., Husted, S., and Wyers, G. P.: Resistance modelling of ammonia exchange over oilseed rape, *Agr. Forest Meteorol.*, 105, 405–425, doi:10.1016/S0168-1923(00)00206-9, 2000.
- 500 Nemitz, E., Milford, C., and Sutton, M. A.: A two-layer canopy compensation point model for describing bi-directional biosphere-atmosphere exchange of ammonia, *Q. J. Roy. Meteor. Soc.*, 127, 815–833, doi:10.1002/qj.49712757306, 2001.
- Nemitz, E., Sutton, M. A., Wyers, G. P., and Jongejan, P. A. C.: Gas-particle interactions above a Dutch heathland: I. Surface exchange fluxes of NH<sub>3</sub>, SO<sub>2</sub>, HNO<sub>3</sub> and HCl, *Atmos. Chem. Phys.*, 4, 989–1005, 505 doi:10.5194/acp-4-989-2004, 2004.
- Nopmongkol, U., Koo, B., Tai, E., Jung, J., Piyachaturawat, P., Emery, C., Yarwood, G., Pirovano, G., Mitsakou, C., and Kallos, G.: Modeling Europe with CAMx for the Air Quality Model Evaluation International Initiative (AQMEII), *Atmos. Environ.*, 53, 177–185, doi:10.1016/j.atmosenv.2011.11.023, 2012.
- Pleim, J. E., Bash, J. O., Walker, J. T., and Cooter, E. J.: Development and evaluation of an ammonia bi-directional flux parametrization for air quality models, *J. Geophys. Res.-Atmos.*, 118, 3794–3806, 510 doi:10.1002/jgrd.50262, 2013.
- Pope, C. A., Ezzati, M., and Dockery, D. W.: Fine-particulate air pollution and life expectancy in the US, *New Engl. J. Med.*, 360, 376–386, doi:10.1056/NEJMsa0805646, 2009.
- Seinfeld, J. H. and Pandis, S. N.: *Atmospheric Chemistry and Physics: From Air Pollution to Climate Change*, 515 2nd edn., J. Wiley, New York, 2006.
- Simpson, D., Benedictow, A., Berge, H., Bergström, R., Emberson, L. D., Fagerli, H., Flechard, C. R., Hayman, G. D., Gauss, M., Jonson, J. E., Jenkin, M. E., Nyíri, A., Richter, C., Semeena, V. S., Tsyro, S., Tuovinen, J.-P., Valdebenito, Á., and Wind, P.: The EMEP MSC-W chemical transport model – technical description, *Atmos. Chem. Phys.*, 12, 7825–7865, doi:10.5194/acp-12-7825-2012, 2012.
- 520 Slinn, S. A. and Slinn, W. G. N.: Predictions for particle deposition on natural waters, *Atmos. Environ.*, 14, 1013–1016, doi:10.1016/0004-6981(80)90032-3, 1980.
- Sutton, M. A., Burkhardt, J. K., Guerin, D., Nemitz, E., and Fowler, D.: Development of resistance models to describe measurements of bi-directional ammonia surface-atmosphere exchange, *Atmos. Environ.*, 32, 473–480, doi:10.1016/S1352-2310(97)00164-7, 1998.
- 525 Taylor, K. E.: Summarizing multiple aspects of model performance in a single diagram, *J. Geophys. Res.*, 106, 7183–7192, doi:10.1029/2000JD900719, 2001.
- Trebs, I., Lara, L. L., Zeri, L. M. M., Gatti, L. V., Artaxo, P., Dlugi, R., Slanina, J., Andreae, M. O., and

- Meixner, F. X.: Dry and wet deposition of inorganic nitrogen compounds to a tropical pasture site (Rondônia, Brazil), *Atmos. Chem. Phys.*, 6, 447–469, doi:10.5194/acp-6-447-2006, 2006.
- 530 UNC: SMOKE V2.4 User's Manual, available at: <http://www.cmascenter.org/smoke/documentation/2.4/html/> (last access: 25 December 2013), 2009.
- Van Bremen, N., Burrough, P. A., Velthorst, E. J., van Dobben, H. F., de Wit, T., Ridder, T. B., and Reijnders, H. F. R.: Soil acidification from atmospheric ammonium sulphate in forest canopy throughfall, *Nature*, 299, 548–550, doi:10.1038/299548a0, 1982.
- 535 Van der Hoven, I.: Deposition of particles and gases, *Meteorology and Atomic Energy*, in: *Meteorology and Atomic Energy*, edited by: Slade, D., US Atomic Energy Commission, 202–208, 1968.
- Vet, R., Li, S.-M., Beaney, G., Belzer, W., Chan, E., Dann, T., Friesen, K., Hayden, K., Hou, A., Iqbal, S., Jones, K., Leithead, A., Liggio, J., Makar, P., Narayan, J., Ro, C.-U., Shaw, M., Sukloff, B., Vingarzan, R., and Qiu, W.: Characterization of ambient ammonia, PM and regional deposition across Canada, Chapter 6,  
540 in: Environment Canada. The 2008 Canadian Atmospheric Assessment of Agricultural Ammonia, Environment Canada, Gatineau, QC, Canada, 93–147, 2008.
- Vieno, M., Dore, A. J., Stevenson, D. S., Doherty, R., Heal, M. R., Reis, S., Hallsworth, S., Tarrason, L., Wind, P., Fowler, D., Simpson, D., and Sutton, M. A.: Modelling surface ozone during the 2003 heat-wave in the UK, *Atmos. Chem. Phys.*, 10, 7963–7978, doi:10.5194/acp-10-7963-2010, 2010.
- 545 Wen, D., Lin, J. C., Meng, F., Gbor, P. K., He, Z., and Sloan, J. J.: Quantitative assessment of upstream source influences on total gaseous mercury observations in Ontario, Canada, *Atmos. Chem. Phys.*, 11, 1405–1415, doi:10.5194/acp-11-1405-2011, 2011.
- Wen, D., Lin, J. C., Millet, D. B., Stein, A. F., and Draxler, R. R.: A backward-time stochastic Lagrangian air quality model, *Atmos. Environ.*, 54, 373–386, doi:10.1016/j.atmosenv.2012.02.042, 2012.
- 550 Wen, D., Lin, J. C., Zhang, L., Vet, R., and Moran, M. D.: Modeling atmospheric ammonia and ammonium using a stochastic Lagrangian air quality model (STILT-Chem v0.7), *Geosci. Model Dev.*, 6, 327–344, doi:10.5194/gmd-6-327-2013, 2013.
- Wesely, M. L.: Parameterization of surface resistance to gaseous dry deposition in regional-scale numerical models, *Atmos. Environ.*, 23, 1293–1304, doi:10.1016/0004-6981(89)90153-4, 1989.
- 555 Wichink Kruit, R. J., Van Pul, W. A. J., Sauter, F. J., Van den Broek, M., Nemitz, E., Sutton, M. A., Krol, M., and Holtslag, A. A. M.: Modeling the surface-atmosphere exchange of ammonia, *Atmos. Environ.*, 44, 945–957, doi:10.1016/j.atmosenv.2009.11.049, 2010.
- Wichink Kruit, R. J., Schaap, M., Sauter, F. J., van Zanten, M. C., and van Pul, W. A. J.: Modeling the distribution of ammonia across Europe including bi-directional surface–atmosphere exchange, *Biogeosciences*, 9,  
560 5261–5277, doi:10.5194/bg-9-5261-2012, 2012.
- Wu, Y., Walker, J., Schwede, D., Peters-Lidard, C., Dennis, R., and Robarge, W.: A new model of bi-directional ammonia exchange between the atmosphere and biosphere: ammonia stomatal compensation point, *Agr. Forest Meteorol.*, 149, 263–280, doi:10.1016/j.agrformet.2008.08.012, 2009.
- Wu, Z., Wang, X., Chen, F., Turnipseed, A. A., Guenther, A. B., Niyogi, D., Charusombat, U., Xia, B.,  
565 Munger, J. W., and Alapaty, K.: Evaluating the calculated dry deposition velocities of reactive nitrogen oxides and ozone from two community models over a temperate deciduous forest, *Atmos. Environ.*, 45, 2663–2674, doi:10.1016/j.atmosenv.2011.02.063, 2011.

- 570 Wu, Z., Wang, X., Turnipseed, A. A., Chen, F., Zhang, L., Guenther, A. B., Karl, T., Huey, L. G., Niyogi, D.,  
Xia, B., and Alapaty, K.: Evaluation and improvements of two community models in simulating dry de-  
position velocities for peroxyacetyl nitrate (PAN) over a coniferous forest, *J. Geophys. Res.-Atmos.*, 117,  
D04310, doi:10.1029/2011JD016751, 2012.
- Zhang, L., Gong, S., Padro, J., and Barrie, L.: A size-segregated particle dry deposition scheme for an atmo-  
spheric aerosol module, *Atmos. Environ.*, 35, 549–560, doi:10.1016/S1352-2310(00)00326-5, 2001.
- 575 Zhang, L., Moran, M., Makar, P., Brook, J., and Gong, S.: Modelling gaseous dry deposition in AU-  
RAMS: a unified regional air-quality modelling system, *Atmos. Environ.*, 36, 537–560, doi:10.1016/S1352-  
2310(01)00447-2, 2002.
- Zhang, L., Brook, J. R., and Vet, R.: A revised parameterization for gaseous dry deposition in air-quality  
models, *Atmos. Chem. Phys.*, 3, 2067–2082, doi:10.5194/acp-3-2067-2003, 2003.
- 580 Zhang, L., Wright, L. P., and Asman, W. A. H.: Bi-directional air-surface exchange of atmospheric ammonia:  
a review of measurements and a development of a big-leaf model for applications in regional-scale air-quality  
models, *J. Geophys. Res.*, 115, D20310, doi:10.1029/2009JD013589, 2010.

**Table 1.** Stomatal and ground emission potential inputs (dimensionless) by land-use category in the ZBE scheme (Zhang et al., 2010). Note that pairs of values correspond to low-N canopies and high-N canopies, respectively.

| Land-use category |                            | Stomatal emission potential<br>$\Gamma_{st}$ | Ground emission potential<br>$\Gamma_g$ |
|-------------------|----------------------------|----------------------------------------------|-----------------------------------------|
| 1                 | Water                      | 0                                            | 0                                       |
| 2                 | Ice                        | 0                                            | 0                                       |
| 3                 | Inland lake                | 0                                            | 0                                       |
| 4                 | Evergreen needleleaf trees | 300, 3000                                    | 20, 1000                                |
| 5                 | Evergreen broadleaf trees  | 300, 3000                                    | 20, 1000                                |
| 6                 | Deciduous needleleaf trees | 300                                          | 200, 2000                               |
| 7                 | Deciduous broadleaf trees  | 300, 3000                                    | 200, 2000                               |
| 8                 | Tropical broadleaf trees   | 300, 3000                                    | 20, 1000                                |
| 9                 | Drought deciduous trees    | 300, 3000                                    | 500, 2000                               |
| 10                | Evergreen broadleaf shrubs | 300, 3000                                    | 20, 1000                                |
| 11                | Deciduous shrubs           | 300, 3000                                    | 200, 1000                               |
| 12                | Thorn shrubs               | 300, 3000                                    | 20, 1000                                |
| 13                | Short grass and forbs      | 300, 3000                                    | 2000, 200 000                           |
| 14                | Long grass                 | 300, 3000                                    | 2000, 100 000                           |
| 15                | Crops                      | 800                                          | 5000                                    |
| 16                | Rice                       | 800                                          | 5000                                    |
| 17                | Sugar                      | 800                                          | 5000                                    |
| 18                | Maize                      | 800                                          | 5000                                    |
| 19                | Cotton                     | 800                                          | 5000                                    |
| 20                | Irrigated crops            | 800                                          | 5000                                    |
| 21                | Urban                      | 0                                            | 0                                       |
| 22                | Tundra                     | 20                                           | 20                                      |
| 23                | Swamp                      | 100                                          | 20                                      |
| 24                | Desert                     | 0                                            | 0                                       |
| 25                | Mixed wood forest          | 300, 3000                                    | 20, 3000                                |
| 26                | Transitional forest        | 300, 3000                                    | 20, 3000                                |

**Table 2.** Definition of statistical metrics.

| Parameter                   | Definition                                                                              |
|-----------------------------|-----------------------------------------------------------------------------------------|
| Ratio of the Means (ROM)    | $\left(\frac{1}{N} \sum_{i=1}^N P_i\right) / \left(\frac{1}{N} \sum_{i=1}^N O_i\right)$ |
| Mean Fractional Bias (MFB)  | $\frac{1}{N} \sum_{i=1}^N \frac{P_i - O_i}{(P_i + O_i)/2} \times 100\%$                 |
| Mean Fractional Error (MFE) | $\frac{1}{N} \sum_{i=1}^N \frac{ P_i - O_i }{(P_i + O_i)/2} \times 100\%$               |

$P_i$ : prediction at time  $i$ ;  $O_i$ : observation at time  $i$ ;  $N$ : total number of observations or predictions.

**Table 3.** Values of three statistical metrics for comparison of weekly modeled  $\text{NH}_3$  concentrations against observations for the 1 June to 30 November 2006 period for three groups of sites: (1) all sites (53); (2) forested sites (14); (3) agricultural sites (39).

| Metrics | All sites |        |       | Agricultural sites |        |       | Forested sites |        |       |
|---------|-----------|--------|-------|--------------------|--------|-------|----------------|--------|-------|
|         | WDD       | ZDD    | ZBE   | WDD                | ZDD    | ZBE   | WDD            | ZDD    | ZBE   |
| ROM     | 0.85      | 0.74   | 1.07  | 0.83               | 0.73   | 1.04  | 1.27           | 0.95   | 1.68  |
| MFB (%) | -2.40     | -24.18 | 23.40 | -14.15             | -26.48 | 12.72 | 32.77          | -17.30 | 55.32 |
| MFE (%) | 56.65     | 52.25  | 57.73 | 48.04              | 50.10  | 49.38 | 82.37          | 58.66  | 82.72 |

**Table 4.** Selected statistics for emission-potential sensitivity tests with the ZBE scheme for five measurement sites with strong anthropogenic  $\text{NH}_3$  emissions. PEP is the pre-defined emission-potential values in Table 1 for land-use categories related to agriculture.

| Tested emission potentials | ROM  | MFB (%) | MFE (%) |
|----------------------------|------|---------|---------|
| 1 $\times$ PEP             | 0.79 | -22.59  | 22.59   |
| 2 $\times$ PEP             | 0.88 | -13.56  | 14.43   |
| 3 $\times$ PEP             | 0.99 | -2.13   | 11.11   |
| 4 $\times$ PEP             | 1.09 | 8.15    | 11.31   |
| 6 $\times$ PEP             | 1.31 | 25.87   | 25.87   |

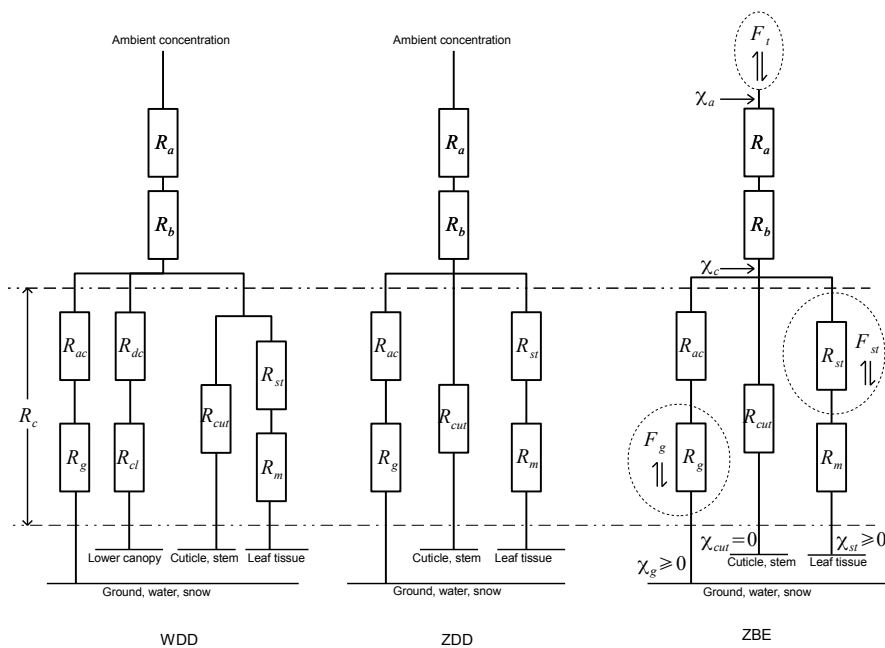


**Fig. 1.** Diagrammatic representation of the WDD, ZDD, and ZBE schemes. Resistances include the aerodynamic resistance ( $R_a$ ), the quasi-laminar sublayer resistance above the canopy ( $R_b$ ), and the overall canopy resistance ( $R_c$ ).  $R_c$  can be decomposed into stomatal resistance ( $R_{st}$ ), mesophyll resistance ( $R_m$ ), in-canopy aerodynamic resistance ( $R_{ac}$ ), soil resistance ( $R_g$ ), cuticle resistance ( $R_{cut}$ ), lower canopy resistance ( $R_{cl}$ ), and resistance for the gas transfer affected by buoyancy convection in the canopy ( $R_{dc}$ ).  $F_t$  is overall flux at a reference height above the canopy.  $F_{st}$  and  $F_g$  are bi-directional fluxes through stomata and above the soil surface, respectively.  $\chi_a$  is the ambient concentration at the reference height.  $\chi_c$  is the concentration at the top of canopy.  $\chi_{st}$  and  $\chi_g$  are the stomatal and soil compensation points, respectively.

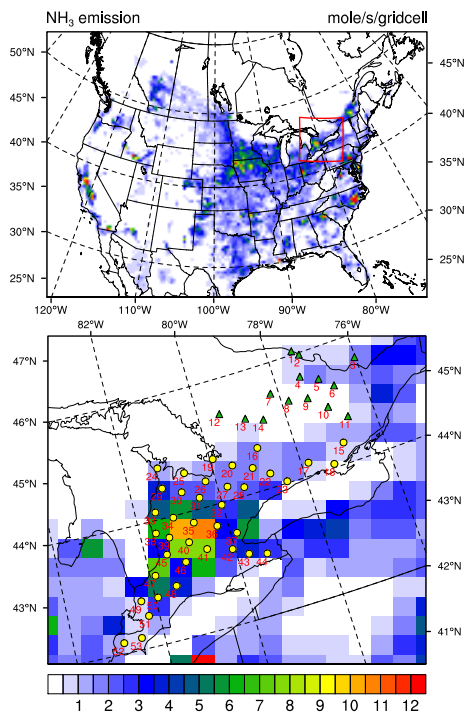


**Fig. 2.** Locations and IDs of 53 measurement sites and spatial distribution of gridded  $\text{NH}_3$  emissions fluxes ( $\text{mols}^{-1}\text{gridcell}^{-1}$ ) over the simulation domain (top panel) and their local  $\text{NH}_3$  emission fluxes (bottom panel) is a magnification of the area enclosed by red lines in the top panel). Measurement sites include 14 forest sites (green triangles) and 39 agricultural sites (yellow dots). Note that the emission fluxes are averages over the entire simulation period.

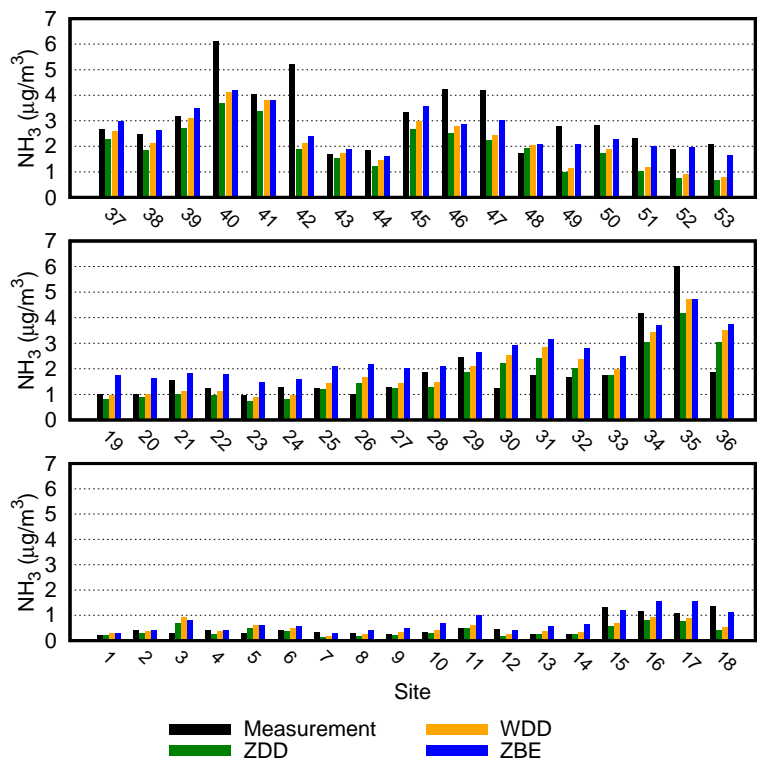


**Fig. 3.** Observed (black) and modeled  $\text{NH}_3$  concentration averages with the WDD scheme (orange), the ZDD scheme (green), and the ZBE scheme (blue) for 53 measurement sites for the 1 June to 30 November 2006 period. Sites 1 to 14 are forest sites.

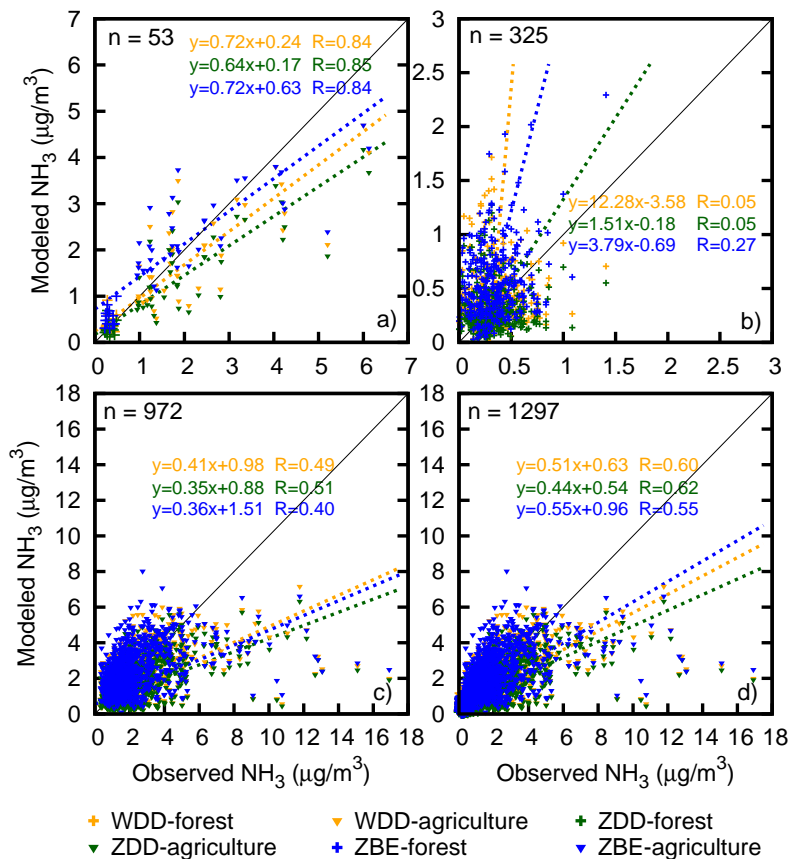


**Fig. 4.** Correlations between measured and modeled  $\text{NH}_3$  concentrations for the WDD (orange), ZDD (green), and ZDD (blue) schemes, respectively, including: (a) for all 53 sites using mean concentrations over the entire simulation period; (b) for forest sites (+) using weekly concentrations; (c) for agricultural sites (▼) using weekly concentrations; (d) for all 53 sites using weekly concentrations. Solid black lines represents 1:1 lines.

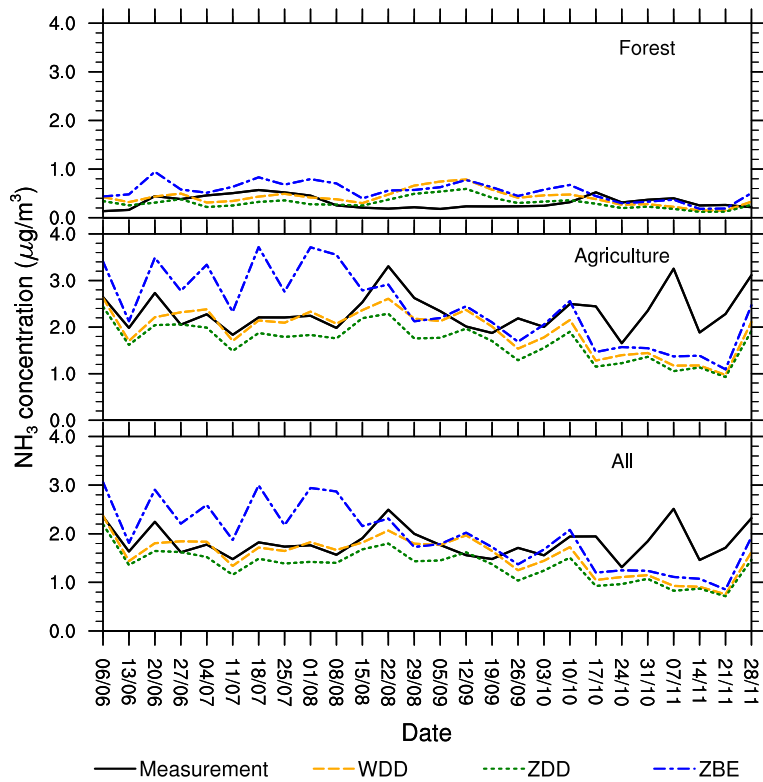


**Fig. 5.** Observed NH<sub>3</sub> concentration time series (black continuous line) vs. modeled time series using the WDD scheme (orange), the ZDD scheme (green), and the ZBE scheme (blue), respectively. Those time series are averages over forest sites (top), agricultural sites (middle), and all 53 sites (bottom).

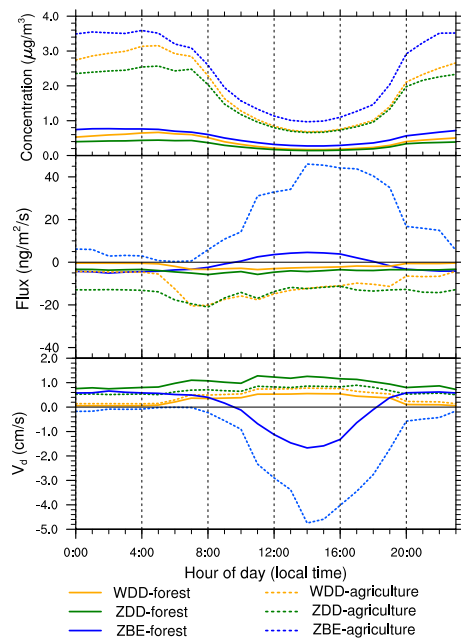


**Fig. 6.** Diurnal variations of modeled dry deposition velocity (bottom), surface exchange flux (middle), and  $\text{NH}_3$  concentration (top) using WDD (orange), ZDD (green), and ZBE (blue) schemes, respectively, averaged over the entire simulation period for forest sites (solid lines) and agricultural sites (dashed lines). Negative fluxes represent downward movement out of the atmosphere whereas positive fluxes represent emission from the Earth's surface to the atmosphere. Dry deposition velocities for ZBE represent its effective dry deposition velocities, where negative values indicate emissions from surface.

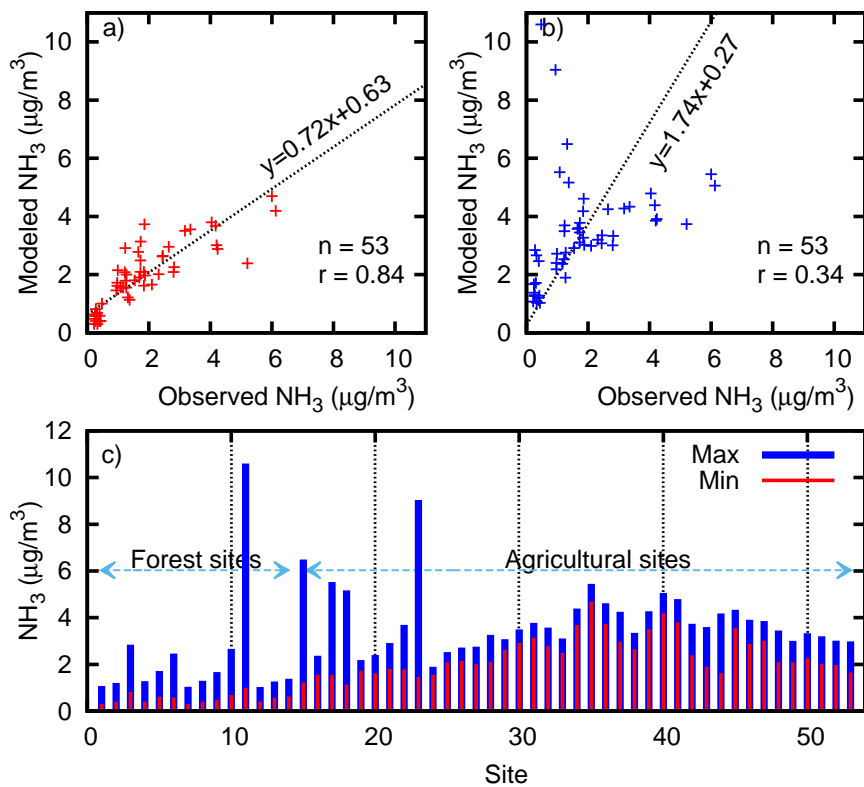


**Fig. 7.** Modeled average  $\text{NH}_3$  concentration using the set of a) minimum emission potentials (red) and using the set of b) maximum emission potentials (blue) for 53 measurement sites (c) and their correlations with the observations (a and b). The use of minimum emission potentials is the default.

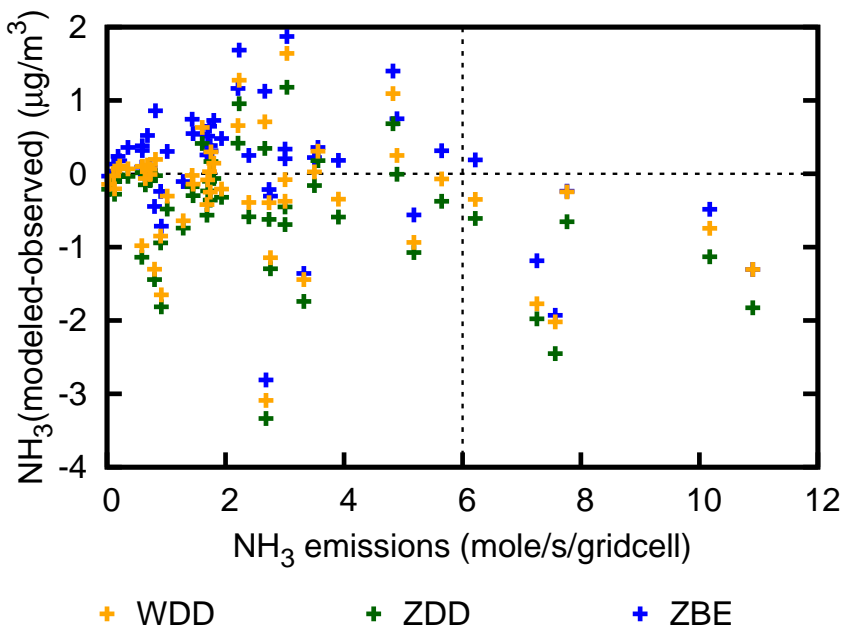


**Fig. 8.** Scatterplot for deviations of modeled NH<sub>3</sub> concentrations from observed values vs. corresponding mean anthropogenic emission strengths for the three schemes for each test sites. All data points are means for the entire simulation period.